

Coulomb drag in graphene near the Dirac point

M. Schütt,¹ P.M. Ostrovsky,^{2,1,3} M. Titov,⁴ I.V. Gornyi,^{1,5} B.N. Narozhny,⁶ and A.D. Mirlin^{1,6,7}

¹*Institut für Nanotechnologie, Karlsruhe Institute of Technology, 76021 Karlsruhe, Germany*

²*Max-Planck-Institut für Festkörperforschung, Heisenbergstr. 1, 70569, Stuttgart, Germany*

³*L.D. Landau Institute for Theoretical Physics RAS, 119334 Moscow, Russia*

⁴*Radboud University Nijmegen, Institute for Molecules and Materials, NL-6525 AJ Nijmegen, The Netherlands*

⁵*A.F. Ioffe Physico-Technical Institute, 194021 St. Petersburg, Russia*

⁶*Institut für Theorie der Kondensierten Materie and DFG Center for Functional Nanostructures, Karlsruher Institut für Technologie, 76128 Karlsruhe, Germany*

⁷*Petersburg Nuclear Physics Institute, 188350 St. Petersburg, Russia*

(Dated: September 14, 2018)

We study Coulomb drag in double-layer graphene near the Dirac point. A particular emphasis is put on the case of clean graphene, with transport properties dominated by the electron-electron interaction. Using the quantum kinetic equation framework, we show that the drag becomes T -independent in the clean limit, $T\tau \rightarrow \infty$, where T is temperature and $1/\tau$ impurity scattering rate. For stronger disorder (or lower temperature), $T\tau \ll 1/\alpha^2$, where α is the interaction strength, the kinetic equation agrees with the leading-order (α^2) perturbative result. At still lower temperatures, $T\tau \ll 1$ (diffusive regime) this contribution gets suppressed, while the next-order (α^3) contribution becomes important; it yields a peak centered at the Dirac point with a magnitude that grows with lowering $T\tau$.

PACS numbers: 72.80.Vp, 73.23.Ad, 73.63.Bd

Frictional drag in double-layer systems consisting of two closely spaced, but electronically isolated conductors is a well established experimental tool for studying the microscopic structure of solids [1–7]. In such an experiment a current I_1 is passed through one of the conductors (the “active” layer) and the induced voltage drop V_2 is measured along the other (“passive”) layer. The ratio of this voltage to the driving current $\rho_D = -V_2/I_1$ (known as the drag coefficient or the transresistivity) is a measure of both the inter-layer interaction [1, 2] and the microscopic state [3–6] of the layers. At low temperatures the drag effect is dominated by direct Coulomb interaction between the carriers in the two layers.

The physics of Coulomb drag is well understood if both layers are in the Fermi liquid state [10, 11]. The electric field in the passive layer is induced by exciting pairs of electron-like and hole-like excitations in a state with finite total momentum. The momentum is transferred from the current-carrying state in the active layer by the inter-layer Coulomb interaction. The inter-layer momentum transfer can be described by the effective relaxation rate τ_D^{-1} . The most basic qualitative features of the drag measurement [1, 10, 11] can already be inferred by estimating τ_D^{-1} with the help of Fermi’s golden rule, where it is crucial to take into account the energy dependence of the density of states (DoS) and/or diffusion coefficient D : indeed, the current-carrying states can be characterized by non-zero total momentum only in the case of electron-hole asymmetry.

The drag coefficient ρ_D and momentum relaxation rate τ_D^{-1} can be related using a simple Drude-like model. Consider the phenomenological equations of motion, assuming for simplicity that both layers are characterized by

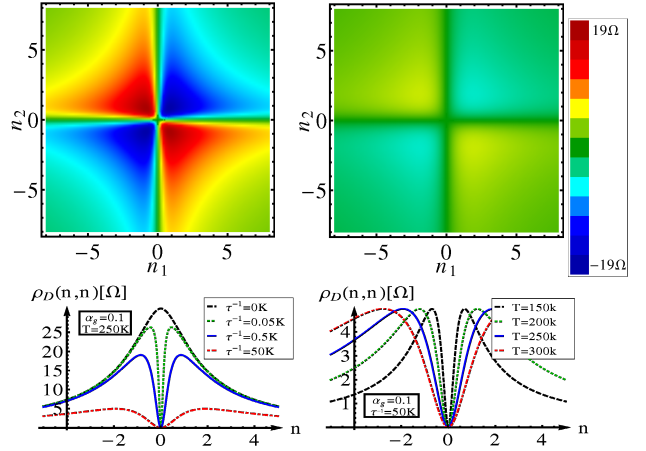


FIG. 1: (Color online) Drag coefficient in the ballistic regime as a function of carrier densities (in units of 10^{11} cm^{-2}) for $d = 9 \text{ nm}$. The left panels show ρ_D at $T = 250 \text{ K}$, with the upper panel corresponding to ultra-clean graphene $\tau^{-1} = 0.5 \text{ K}$ and the lower left panel showing the evolution of ρ_D with increasing disorder from $\tau^{-1} = 0$ to $\tau^{-1} = 50 \text{ K}$. The right panels show ρ_D for $\tau^{-1} = 50 \text{ K}$. The four curves on the lower panel correspond to $T = 150 \text{ K}$, 200 K , 250 K , and 300 K .

the same carrier density n and effective mass m

$$\frac{d}{dt} \begin{pmatrix} \mathbf{j}_1 \\ \mathbf{j}_2 \end{pmatrix} = \frac{e^2 n}{m} \begin{pmatrix} \mathbf{E}_1 \\ \mathbf{E}_2 \end{pmatrix} - \frac{1}{\tau_D} \begin{pmatrix} 1 & -1 \\ -1 & 1 \end{pmatrix} \begin{pmatrix} \mathbf{j}_1 \\ \mathbf{j}_2 \end{pmatrix} - \frac{1}{\tau} \begin{pmatrix} \mathbf{j}_1 \\ \mathbf{j}_2 \end{pmatrix}, \quad (1)$$

where $\mathbf{j}_{1(2)}$ is the average current density in the active (passive) layer, $\mathbf{E}_{1(2)}$ is the electric field in the two layers, and τ is the impurity scattering time. Noting that in the drag measurement no net current is allowed to flow in the

passive layer $j_2 = 0$, we arrive at the Drude-like formula

$$\rho_D = -\rho_{12} = (e^2 n \tau_D / m)^{-1}. \quad (2)$$

Combining Eq. (2) with the Fermi's golden rule estimate for τ_D^{-1} one can estimate the drag coefficient. More rigorous calculations based on either the diagrammatic perturbation theory [10] or the kinetic equation [11] confirm the ‘‘Fermi-liquid’’ result

$$\rho_D^{FL} = (\hbar/e^2) A_{12} T^2 / (\mu_1 \mu_2), \quad (3)$$

where $\mu_{1(2)}$ is the chemical potential of the active (passive) layer and A_{12} is determined by the matrix elements of the inter-layer interaction (the precise form of A_{12} as a function of the inter-layer spacing d depends on whether transport in the two layers is ballistic or diffusive [10]).

Even though the drag coefficient (3) is apparently independent of the impurity scattering time τ , transport properties of each individual layer are usually [1, 10] assumed to be dominated by disorder, $\tau \ll \tau_D$. In particular, solving Eq. (1) for the resistivity one finds the usual Drude formula. In contrast, the behavior of clean double-layer systems, i.e. with $\tau \gg \tau_D$, is less trivial. In this case, the last term in Eq. (1) may be neglected leading to the non-zero result for the single-layer resistivity

$$\rho_{11} = -\rho_{12} = (e^2 n \tau_D / m)^{-1} = \rho_D. \quad (4)$$

Note, that the system is still characterized by the infinite conductivity ($\hat{\rho}^{-1} = \infty$), as expected for disorder-free conductors on the grounds of Galilean invariance.

The physical picture of the drag effect outlined so far is based on the following assumptions: (i) each of the layers is assumed to be in a Fermi-liquid state, which at the very least means $\mu_{1(2)} \gg T$; (ii) electron-electron interaction does not contribute to the transport scattering time; (iii) the inter-layer Coulomb interaction is assumed to be weak enough, $\alpha = e^2 / (\hbar v_F) \ll 1$, such that ρ_D is determined by the lowest-order perturbation theory [10].

Lifting one or more of the above assumptions leads to significant changes in the drag effect [3–5, 7–9]. In this Letter we focus on the system of two parallel graphene sheets [7–9, 12–21], which offers a great degree of control over the microscopic structure of the two layers. Indeed, using hexagonal boron nitride as a substrate [9, 22], one can decrease disorder strength in the system and reach the regime, where transport properties of the two layers are dominated by electron-electron interaction, $\tau \gg \tau_{ee}$. Moreover, the carrier density can be electrostatically controlled allowing one to scan a wide range of chemical potentials from the Fermi liquid regime to the Dirac point.

While inapplicable to massless fermions in graphene, the equations of motion (1) provide an expectation of non-zero resistance in the case of the ultra-clean system. Below, we use the quantum kinetic equation (QKE) approach [23, 24] to derive hydrodynamic equations [25]

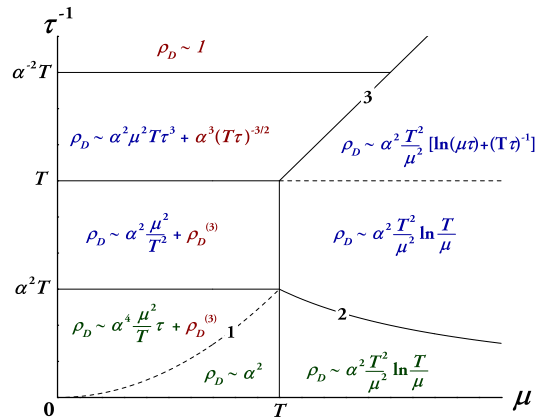


FIG. 2: (Color online) Drag coefficient in the case of identical layers in different parameter regimes for $\mu \ll \min(T/\alpha, v/d)$. The bottom row of results (for $\tau^{-1} \ll \alpha^2 T$ and below the curve 2, $\tau^{-1} \ll \alpha^2 T^2/\mu$) are obtained from the solution of the QKE (13). The curve 1 ($\tau^{-1} = \alpha^2 \mu^2/T$) separates the two regimes in Eq. (15). The middle row of results (for $\alpha^2 T \ll \tau^{-1} \ll T$) corresponds to the region where the results and the applicability of the QKE overlap with those of the perturbation theory of Ref. 16 (for $\mu \gg T$ the results above and below the curve 2 contain different numerical factors). The third-order contribution $\rho_D^{(3)} = \mathcal{O}(\alpha^3)$ resulting in small non-zero drag at $\mu = 0$ is shown in red. The upper row of results ($\tau^{-1} \gg T$) corresponds to the diffusive regime [see Eqs. (17) and (18)], where $\rho_D^{(3)}$ saturates for $\tau^{-1} \gg T/\alpha^2$.

that generalize Eq. (1) for interacting Dirac fermions in graphene. Solving these equations (or equivalently, the QKE) we confirm that the system of two ultra-clean graphene sheets is indeed characterized by a non-zero, but degenerate resistance matrix whose elements satisfy Eq. (4), with ρ_D shown in Fig. 1.

Kinetic equation. — We now briefly outline the derivation of the QKE for double-layer graphene structures and its solution in the ballistic regime (see Supplemental Material [27]). Consider an infinite sample in an infinitesimal, homogeneous electric field \mathbf{E}_1 applied to the active layer. The response of the system to the field can be described by the small non-equilibrium corrections $h_{1(2)}$ to the Fermi distribution functions defined by

$$n_i(\epsilon, \hat{\mathbf{v}}) = n_F^{(i)}(\epsilon) + T \frac{\partial n_F^{(i)}(\epsilon)}{\partial \epsilon} h_i(\epsilon, \hat{\mathbf{v}}), \quad (5)$$

where the eigenstates of the Dirac Hamiltonian $H = v \sigma \mathbf{p}$ are labeled [27] by their energy ϵ and the velocity unit vector $\hat{\mathbf{v}}$; the momentum of the particle is $\mathbf{p} = \epsilon \hat{\mathbf{v}}/v$.

Small corrections $h_{1(2)}$ can be found by linearizing the QKE [26]

$$\begin{aligned} \frac{\partial h_1}{\partial t} + \frac{e \mathbf{E}_1 \mathbf{v}}{T} &= -\frac{h_1}{\tau} + I_{11}\{h_1\} + I_{12}\{h_1, h_2\}, \\ \frac{\partial h_2}{\partial t} &= -\frac{h_2}{\tau} + I_{22}\{h_2\} + I_{21}\{h_2, h_1\}, \end{aligned} \quad (6)$$

where the linearized pair-collision integrals are given by

$$I_{ij} = - \int d2 d3 d4 W^{ij}(h_{i,1} - h_{i,2} + h_{j,3} - h_{j,4}),$$

$$W^{ij} = \delta(\mathbf{p}_1 - \mathbf{p}_2 + \mathbf{p}_3 - \mathbf{p}_4) \delta(\epsilon_1 - \epsilon_2 + \epsilon_3 - \epsilon_4)$$

$$\times \frac{\cosh \frac{\epsilon_1 - \mu_i}{2T}}{2 \cosh \frac{\epsilon_2 - \mu_i}{2T} \cosh \frac{\epsilon_3 - \mu_j}{2T} \cosh \frac{\epsilon_4 - \mu_j}{2T}} K_{1,2;3,4}^{ij}, \quad (7)$$

and we have used short-hand notations $h_{i,a} = h(\epsilon_a, \hat{\mathbf{v}}_a)$, $da = \nu(\epsilon_a) d\hat{\mathbf{v}}_a d\epsilon_a$, with $a = 1, 2, 3, 4$. The kernel

$$K_{1,2;3,4}^{ij} = |U^{ij}(\mathbf{p}_1 - \mathbf{p}_2)|^2 \frac{1 + \hat{\mathbf{v}}_1 \hat{\mathbf{v}}_2}{2} \frac{1 + \hat{\mathbf{v}}_3 \hat{\mathbf{v}}_4}{2}, \quad (8)$$

contains the interaction matrix element describing the two-particle scattering $1 \rightarrow 2$ and $3 \rightarrow 4$ and the corresponding Dirac factors. Here we take into account only the Hartree interaction term: there is no exchange interaction between the layers, whereas within the layers the Hartree term dominates in the large- N limit (N is the number of electron flavors; physically, $N = 4$ due to spin and valley degeneracy).

The peculiarity of the inelastic scattering in the Dirac spectrum is two-fold. First, since the velocity $\mathbf{v} = v^2 \mathbf{p} / \epsilon$ is independent of the absolute value of the momentum, total momentum conservation does not prevent velocity (or current) relaxation. As a result, the intralayer collision integral I_{ij} yields a non-zero transport relaxation rate due to electron-electron scattering.

Second, the scattering of particles with almost collinear momenta is enhanced since the momentum and energy conservation laws coincide for collinear scattering. This restricts the kinematics [23, 24, 28] of the Dirac fermions leading to the singularity in the collision integral. This singularity leads to the fast thermalization of particles within a given direction, which justifies the Ansatz:

$$h_i(\epsilon, \hat{\mathbf{v}}) = \left(\chi_v^{(i)} + \chi_p^{(i)} \epsilon / T \right) e \mathbf{E} \mathbf{v} / T^2. \quad (9)$$

The Ansatz (9) retains the only two modes for which the collision integral I_{ij} is not singular: the ‘‘momentum mode’’ $\chi_p^{(i)}$, which nullifies the collision integral due to momentum conservation, and the ‘‘velocity mode’’ $\chi_v^{(i)}$, which nullifies I_{ij} in the case of collinear scattering. The same kinematic restrictions lead to fast uni-directional thermalization between the layers. This allows us to set $\chi_p^{(1)} = \chi_p^{(2)}$, and hence reduce the QKE for the double-layer setup to a 3×3 matrix equation.

Consider for simplicity the case of identical layers (for the more general case of $\mu_1 \neq \mu_2$ see Supplemental Material [27]). Integrating the reduced QKE over the energies, we arrive at the set of steady-state hydrodynamic equations in terms of the particle currents

$$\mathbf{J}_i = -NT \int d\epsilon \nu(\epsilon) \frac{\partial n_F^{(i)}}{\partial \epsilon} \int d\hat{\mathbf{v}} \mathbf{v} h_i(\epsilon, \hat{\mathbf{v}}), \quad (10)$$

and the total momentum $\mathbf{P} = e\epsilon_0 C_1^2 (\mathbf{E}_1 + \mathbf{E}_2) \tau$:

$$e\epsilon_0 \begin{pmatrix} \mathbf{E}_1 \\ \mathbf{E}_2 \end{pmatrix} = \left[\frac{1}{\tau} + \hat{\mathcal{I}}_{ee} - \hat{\mathcal{I}}_D \right] \begin{pmatrix} \mathbf{J}_1 \\ \mathbf{J}_2 \end{pmatrix} + \left[\frac{1}{\tau_D} - \frac{1}{\tau_{ee}} \right] \begin{pmatrix} \mathbf{P} \\ \mathbf{P} \end{pmatrix}, \quad (11)$$

where $\hat{\mathcal{I}}_{ee(D)} = [(\hat{\sigma}_0 + \hat{\sigma}_1)C_1^2 + 2\hat{\sigma}_{0(1)}C_2] / \tau_{ee(D)}$, the intra- and inter-layer electron-electron transport scattering rates are ($\mathcal{W}^{ij} = W^{ij} \nu_1 / \cosh^2[(\epsilon_1 - \mu_i)/(2T)]$)

$$\frac{1}{\tau_D} = \frac{1}{4T\epsilon_0 C_2} \int \prod_{a=1}^4 da \mathcal{W}^{12}(\mathbf{v}_1 - \mathbf{v}_2)(\mathbf{v}_4 - \mathbf{v}_3),$$

$$\frac{1}{\tau_{ee}} = \frac{1}{8T\epsilon_0 C_2} \int \prod_{a=1}^4 da \left[\mathcal{W}^{11}(\mathbf{v}_1 - \mathbf{v}_2 + \mathbf{v}_3 - \mathbf{v}_4)^2 \right. \\ \left. + 2\mathcal{W}^{12}(\mathbf{v}_1 - \mathbf{v}_2)^2 \right], \quad (12)$$

and σ_k are the Pauli matrices in ‘‘layer space’’. The coefficients $C_{1(2)}$ represent the average energy and energy variation, while $\epsilon_0 = 2T \mathcal{J}\{1\} / N$ is a typical energy:

$$C_1 = \frac{\langle \epsilon \rangle_\epsilon}{T} \sim \frac{\mu}{T}, \quad C_2 = \frac{\langle \epsilon^2 \rangle_\epsilon - \langle \epsilon \rangle_\epsilon^2}{T^2} \sim const,$$

$$\mathcal{J}\{\dots\} = -\frac{v^2}{T} \int d\epsilon \nu(\epsilon) \frac{\partial n_F}{\partial \epsilon} \dots, \quad \langle \dots \rangle_\epsilon = \frac{\mathcal{J}\{\dots\}}{\mathcal{J}\{1\}}.$$

The hydrodynamic equations (11) generalize the equations of motion (1) to the case of Dirac fermions in graphene. The kinematic peculiarity of Dirac fermions manifests itself in the appearance of the total momentum, which entangles the electric fields in the two layers.

Solving the hydrodynamic equations (11) we find

$$\rho_D = \frac{\hbar C_2 (\tau \tau_D)^{-1} + C_1^2 [\tau_{ee}^{-2} - \tau_D^{-2}]}{e^2 \epsilon_0 \tau^{-1} + C_1^2 [\tau_{ee}^{-1} - \tau_D^{-1}]}. \quad (13)$$

For a clean system, the resistivity matrix is degenerate and the drag coefficient is given by

$$\rho_D(\tau \rightarrow \infty) = (\hbar/e^2)(C_2/\epsilon_0) (\tau_D^{-1} + \tau_{ee}^{-1}), \quad (14)$$

which remains non-zero $\rho_D \sim (\hbar/e^2)\alpha^2$ even at the Dirac point $\mu = 0$, where it is determined by $\tau_{ee}^{-1} \sim \alpha^2 T$ (to the second order in the inter-layer interaction $\tau_D^{-1}(\mu = 0) = 0$, while the third-order contribution $\tau_D^{-1}(\mu = 0) \sim \alpha^3 T$ is subleading; the latter is expected to dominate the effect for sufficiently strong disorder, see below).

Equation (13) gives the general expression for the drag coefficient in the ballistic regime based on the solution of the QKE (6). For arbitrary parameter values this expression is to be evaluated numerically (see Fig. 1 for the numerical results). Analytical expressions can be obtained for various limiting cases (summarized in Fig. 2). Below, we discuss the asymptotic behavior of ρ_D for the case of two inequivalent layers [27] focusing on the experimentally relevant case [7–9] $Td/v < 1$ and analyzing the evolution of ρ_D with increasing disorder strength.

Ballistic regime. — For weak disorder $\alpha^2 T \tau \gg 1$ (or $\tau^{-1} \ll \tau_{ee}^{-1}$) and neglecting the third-order contribution to τ_D^{-1} , we find for ρ_D near the Dirac point

$$\rho_D(\mu_i \ll T) \approx 2.87 \frac{\hbar}{e^2} \alpha^2 \frac{\mu_1 \mu_2}{\mu_1^2 + \mu_2^2 + 0.49T/(\alpha^2 \tau)}, \quad (15)$$

where $\tau_D^{-1} \sim \alpha^2 \mu_1 \mu_2 / T$, $\tau_{ee}^{-1} \sim \alpha^2 T$, $\epsilon_0 \sim T$, and $C_2 \sim 1$. The value of ρ_D precisely at the Dirac point depends on the experimental set-up. For clean samples, if one of the chemical potentials remains non-zero, while the other is scanned through the Dirac point [7], then $\rho_D(\mu_1 = 0, \mu_2 \neq 0) = 0$, similar to Ref. 8. On the contrary, if both chemical potentials are driven through the Dirac point simultaneously [9], then Eq. (15) predicts a non-vanishing value of $\rho_D(\mu_1 = \pm \mu_2 = 0) \neq 0$, see Fig. 1.

For intermediate disorder strength $\alpha^2 T \ll \tau^{-1} \ll T$ the applicability region of the QKE overlaps with that of the conventional perturbation theory developed in Ref. 16 and we recover perturbative results, see Fig. 2.

For even stronger disorder (or at low temperatures) $T \tau \ll 1$ the electron motion becomes diffusive. In this case the kinematic restrictions are relaxed and the Ansatz (9) is no longer justified. However, in this regime, the perturbative approach is applicable and allows for a standard description of the diffusive transport.

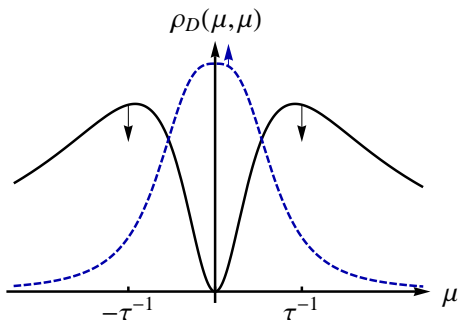


FIG. 3: (Color online) Schematic view of the drag coefficient at low temperatures: the second-order contribution $\rho_D^{(2)}$ (solid line) and the third-order contribution $\rho_D^{(3)}$ (blue dashed line). The arrows indicate the tendency of the two terms with the decrease of temperature $T \rightarrow 0$.

Diffusive regime. — The lowest-order perturbative calculation [10] amounts to evaluation of the Aslamasov-Larkin-type diagram for the drag conductivity given by

$$\sigma_D^{\alpha\beta} = \frac{1}{16\pi T} \sum_{\mathbf{q}} \int \frac{d\omega}{\sinh^2 \frac{\omega}{2T}} \Gamma_1^\beta(\omega, \mathbf{q}) \Gamma_2^\alpha(\omega, \mathbf{q}) |\mathcal{D}_{12}^R|^2, \quad (16)$$

where \mathcal{D}_{12}^R is the retarded propagator of the inter-layer interaction and $\Gamma_a^\alpha(\omega, \mathbf{q})$ is the non-linear susceptibility [in fact, all previous studies of the Coulomb drag in graphene [12–20] focused on Eq. (16)]. In the diffusive regime,

$\Gamma_a^\alpha(\omega, \mathbf{q})$ can be found using the Ohm's law and the continuity equation [30] $\mathbf{\Gamma} = e\mathbf{q}(\partial\sigma/\partial n)\text{Im}\Pi^R$. All microscopic details are now encoded in the diffusion coefficient and the density dependence of the single-layer conductivity σ . Close to the Dirac point $\mu \ll T \ll \tau^{-1}$ the derivative $\partial\sigma/\partial n \sim nv^2\tau^2$ (independently of the precise nature of impurities). After this the evaluation of Eq. (16) is rather standard (except that, in contrast to Ref. 10, the Thomas-Fermi screening length is much longer than the inter-layer spacing $\kappa d \ll 1$) and yields

$$\rho_D^{(2)}(\mu_i \ll T \ll \tau^{-1}) \sim (\hbar/e^2)\alpha^2 \mu_1 \mu_2 T \tau^3. \quad (17)$$

This result vanishes at the Dirac point as a consequence of the electron-hole symmetry.

The importance of the electron-hole asymmetry for the Coulomb drag follows from Eq. (16): the non-linear susceptibility can be thought of as a measure of the asymmetry. However, Eq. (16) is only the lowest-order contribution to σ_D . Under standard assumptions of the Fermi-liquid behavior in the two layers ($\mu \gg v/d \gg T$, $\mu\tau \gg 1$), this contribution indeed dominates the observable effect. On the contrary, in the vicinity of the Dirac point in graphene, the next-order contribution $\rho_D^{(3)}$ [29] becomes important since it is insensitive to the electron-hole symmetry and thus does not vanish at the Dirac point.

The explicit results of Ref. 29 were obtained in the usual limit $\kappa d \gg 1$. Extending these calculations to the opposite case $\kappa d \ll 1$ we find close to the Dirac point

$$\rho_D^{(3)}(\mu_i \ll T \ll \tau^{-1} \ll \alpha^{-2}T) \sim (\hbar/e^2)\alpha^3 (T\tau)^{-3/2}, \quad (18)$$

and $\rho_D^{(3)} \sim \hbar/e^2$ for $\tau^{-1} \gg \alpha^{-2}T$. Away from the Dirac point this contribution decays as a function of the chemical potential $\rho_D^{(3)}(\mu\tau \gg \max[1, \alpha^{-1}(T\tau)^{1/2}]) \sim (\hbar/e^2)(\mu\tau)^{-3}$ and rapidly becomes subleading. As a result, $\rho_D^{(3)}$ is only detectable at low T and μ , see Fig. 3.

While estimating $\rho_D^{(3)}$ at the Dirac point, we assume the single-layer conductivity $\sigma \sim e^2/h$ discarding localization effects. Indeed, experiments on high-quality samples show T -independent σ down to $T = 30$ mK [31], that can be explained by the specific character of disorder in graphene [32].

Summary. — We have studied Coulomb drag in double-layer graphene structures. By using the QKE formalism we have shown that for weak disorder (or high T ; ballistic regime) ρ_D near the Dirac point is given by Eq. (15), see also Fig. 1, which is consistent with Ref. 8. For $\alpha^2 T \tau \ll 1$, the solution of the QKE agrees with the perturbative calculation of Ref. 16. For even stronger disorder (or lower T ; diffusive regime) subleading third-order contribution dominates the effect in qualitative agreement with the experimentally observed peak at the Dirac point at low temperatures [9]. A possible alternative origin of the low- T peak at the Dirac point is a collective state of the double-layer system, either due

to strong interaction [33] (not explored here) or correlated disorder [34, 35] (discussed in Supplemental Material [27]).

Acknowledgements. — We thank A.K. Geim, K.S. Novoselov, and L. Ponomarenko for communicating their experimental results prior to publication. We are grateful to J. Schmalian and L. Fritz for stimulating discus-

sions. This research was supported by the Center for Functional Nanostructures and SPP 1459 “Graphene” of the Deutsche Forschungsgemeinschaft (DFG), and by BMBF. M.T. is grateful to KIT for hospitality. After this work was completed, we became aware of a closely related studies by J. Lux and L. Fritz [36].

Coulomb drag in graphene near the Dirac point: Supplemental Material

1. Kinetic equation approach

In this section we provide details of derivation of the resistivity tensor in double layer graphene from the kinetic equation approach.

A. Kinetic equation

Eigenstates of the massless Dirac Hamiltonian $H = v\sigma\mathbf{p}$ are characterized by the values of momentum \mathbf{p} and the discrete variable $\chi = \pm 1$ indexing conduction and valence bands. In this representation, energy and velocity are $\epsilon = \alpha v|\mathbf{p}|$ and $\mathbf{v} = \chi v\mathbf{p}/p$. It is, however, more convenient to label the eigenstates by their energy ϵ and the unit velocity vector $\hat{\mathbf{v}}$. The momentum of the particle is then $\mathbf{p} = \epsilon\hat{\mathbf{v}}/v$ and the normalization of the states reads

$$\int \frac{|\epsilon| d\epsilon d\hat{\mathbf{v}}}{(2\pi v)^2} |\epsilon, \hat{\mathbf{v}}\rangle \langle \epsilon, \hat{\mathbf{v}}| = 1. \quad (19)$$

We consider an infinite double-layer graphene sample (layers 1 and 2) in a homogeneous electric field \mathbf{E}_1 applied to the active layer 1. Assuming weak electric field, we start with the linearized kinetic equation:

$$\begin{aligned} \frac{\partial h_1}{\partial t} + \frac{e\mathbf{E}_1\mathbf{v}}{T} &= -\frac{h_1}{\tau} + I_{11}\{h_1\} + I_{12}\{h_1, h_2\}, \\ \frac{\partial h_2}{\partial t} &= -\frac{h_2}{\tau} + I_{22}\{h_2\} + I_{21}\{h_2, h_1\}. \end{aligned} \quad (20)$$

Here the nonequilibrium correction h_i to the Fermi distribution function is defined by

$$n_i(\epsilon, \hat{\mathbf{v}}) = n_F(\epsilon) + T \frac{\partial n_F(\epsilon)}{\partial \epsilon} h_i(\epsilon, \hat{\mathbf{v}}), \quad (21)$$

and I_{ij} is the linearized pair-collision integral:

$$I_{ij} = -N \int d\epsilon_2 d\epsilon_3 d\epsilon_4 \int d\hat{\mathbf{v}}_2 d\hat{\mathbf{v}}_3 d\hat{\mathbf{v}}_4 \nu(\epsilon_2) \nu(\epsilon_3) \nu(\epsilon_4) W^{ij}(1, 3; 2, 4) [(h_i(\epsilon_1, \mathbf{v}_1) - h_i(\epsilon_2, \mathbf{v}_2) + h_j(\epsilon_3, \mathbf{v}_3) - h_j(\epsilon_4, \mathbf{v}_4)], \quad (22)$$

$$W^{ij}(1, 2; 3, 4) = \delta(\mathbf{p}_1 - \mathbf{p}_2 + \mathbf{p}_3 - \mathbf{p}_4) \delta(\epsilon_1 - \epsilon_2 + \epsilon_3 - \epsilon_4) \frac{\cosh \frac{\epsilon_1 - \mu_i}{2T}}{2 \cosh \frac{\epsilon_2 - \mu_i}{2T} \cosh \frac{\epsilon_3 - \mu_j}{2T} \cosh \frac{\epsilon_4 - \mu_j}{2T}} K^{ij}(1, 2; 3, 4). \quad (23)$$

Here $\nu(\epsilon)$ is the density of states for one of N flavors (per spin and per valley in graphene, where $N = 4$). We assume formally the large N limit and neglect the intralayer exchange interaction. We further assume that the scattering does not mix flavors (i.e., we neglect the intervalley scattering due to Coulomb interaction): states 1(3) and 2(4) belong to the same flavor, which gives the overall factor N . The kernel

$$K^{ij}(1, 2; 3, 4) = |M^{ij}|^2 \frac{1 + \hat{\mathbf{v}}_1 \hat{\mathbf{v}}_2}{2} \frac{1 + \hat{\mathbf{v}}_3 \hat{\mathbf{v}}_4}{2} \quad (24)$$

contains the interaction matrix element M_{ij} describing the collision of two particles $1 \rightarrow 2$ and $3 \rightarrow 4$ and the corresponding Dirac factors. Within the Golden-rule approximation, this matrix element is given by the Fourier component of the interaction potential:

$$M_{ij}^{(1)} = U_{ij}^{(0)}(\mathbf{p}_1 - \mathbf{p}_2), \quad (25)$$

where

$$\hat{U}^{(0)}(q) = V_0(q) \begin{pmatrix} 1 & e^{-qd} \\ e^{-qd} & 1 \end{pmatrix}, \quad (26)$$

with

$$V_0(q) = \frac{2\pi e^2}{q}. \quad (27)$$

Further, one can generalize the collision integral to the case of the RPA-screened interaction. Then

$$M_{ij} = U_{ij}^{\text{RPA}}(\mathbf{p}_1 - \mathbf{p}_2, vp_1 - vp_2), \quad (28)$$

where

$$\begin{aligned} \hat{U}^{\text{RPA}}(\mathbf{q}, \omega) &= \frac{V_0(q)}{[1 + V_0(q)\Pi_1(q, \omega)][1 + V_0(q)\Pi_2(q, \omega)] - e^{-2qd}V_0^2(q)\Pi_1(q, \omega)\Pi_2(q, \omega)} \\ &\times \begin{pmatrix} 1 + V_0(q)\Pi_2(q, \omega) & e^{-qd} \\ e^{-qd} & 1 + V_0(q)\Pi_1(q, \omega) \end{pmatrix} (1 - e^{-2qd}), \end{aligned} \quad (29)$$

where $\Pi_i(q, \omega)$ is the polarization operator in layer i .

We will focus on the experimentally relevant case of closely located layers, $Td/v \ll 1$. Furthermore, here we will restrict our consideration to the case of relatively low concentrations, such that $\mu d/v \ll 1$ (the situation with large interlayer distance will be considered in detail elsewhere). Under these conditions we can set $d = 0$ in the interaction matrix elements so that the intralayer and interlayer interactions are just the same. We further assume that the interaction coupling constant is small

$$\alpha = \frac{e^2}{v} \ll 1. \quad (30)$$

For simplicity, we treat impurity scattering within the relaxation time approximation with an energy-independent transport time τ . Generalization to the more realistic case of Coulomb impurities with an energy-dependent transport time will be discussed elsewhere.

B. Collinear-scattering singularity

The momentum and energy conservation establishes severe kinematic restrictions on the scattering in systems with linear spectrum [23]. This can be easily seen, when one rewrites the product of delta-functions in Eq. (23) as integrals over $\mathbf{q} = \mathbf{p}_1 - \mathbf{p}_2$, $\omega = \epsilon_1 - \epsilon_2$, and two angles $\phi_{1(3)}$ between \mathbf{q} and $\mathbf{p}_{1(3)}$, respectively:

$$\begin{aligned} \delta(\mathbf{v}_1\epsilon_1 - \mathbf{v}_2\epsilon_2 + \mathbf{v}_3\epsilon_3 - \mathbf{v}_4\epsilon_4) &= \int \frac{d^2q}{(2\pi)^2} \delta(\mathbf{v}_1\epsilon_1 - \mathbf{v}_2\epsilon_2 - \mathbf{q}) \delta(\mathbf{v}_3\epsilon_3 - \mathbf{v}_4\epsilon_4 + \mathbf{q}), \\ \delta(\epsilon_1 - \epsilon_2 + \epsilon_3 - \epsilon_4) &= \int_{-\infty}^{\infty} d\omega \delta(\epsilon_1 - \epsilon_2 - \omega) \delta(\epsilon_3 - \epsilon_4 + \omega), \end{aligned} \quad (31)$$

This allows one to integrate out \mathbf{p}_2 and \mathbf{p}_4 ($\mathbf{v}_{2,4}$ and $\epsilon_{2,4}$) in the collision integral, leading to the product

$$\delta(\epsilon_1 - \omega - \sqrt{\epsilon_1^2 + q^2v^2 - 2\epsilon_1qv \cos \phi_1}) \delta(\epsilon_3 + \omega - \sqrt{\epsilon_3^2 + q^2v^2 + 2\epsilon_3qv \cos \phi_3}), \quad (32)$$

which sets

$$\epsilon_1 - \omega = v|\mathbf{p}_1 - \mathbf{q}| \Rightarrow \cos \phi_1 = \frac{q^2 v^2 - \omega^2 + 2\epsilon_1 \omega}{2\epsilon_1 q v}, \quad (33)$$

$$\epsilon_3 + \omega = |\mathbf{p}_3 + \mathbf{q}| \Rightarrow \cos \phi_3 = \frac{\omega^2 - q^2 v^2 + 2\epsilon_3 \omega}{2\epsilon_3 q v}. \quad (34)$$

When calculating the scattering rates using the collision integral (22), the angular integration over ϕ_1 and ϕ_3 removes the delta-functions, producing the factor

$$\frac{\epsilon_1 - \omega}{\epsilon_1 q v |\sin \phi_1|} \frac{\epsilon_3 + \omega}{\epsilon_3 q v |\sin \phi_3|} = \frac{4(\epsilon_1 - \omega)(\epsilon_3 + \omega)}{(q^2 v^2 - \omega^2) \sqrt{[(2\epsilon_1 - \omega)^2 - q^2 v^2][(2\epsilon_3 + \omega)^2 - q^2 v^2]}}. \quad (35)$$

In combination with the Dirac factors from Eq. (24),

$$(1 + \mathbf{v}_1 \mathbf{v}_2)(1 + \mathbf{v}_3 \mathbf{v}_4) = \frac{(2\epsilon_1 - \omega)^2 - q^2 v^2}{2\epsilon_1(\epsilon_1 - \omega)} \frac{(2\epsilon_3 + \omega)^2 - q^2 v^2}{2\epsilon_3(\epsilon_3 + \omega)}, \quad (36)$$

this yields

$$\frac{1}{q^2 v^2 - \omega^2} \frac{\sqrt{(2\epsilon_1 - \omega)^2 - q^2 v^2}}{\epsilon_1} \frac{\sqrt{(2\epsilon_3 + \omega)^2 - q^2 v^2}}{\epsilon_3}. \quad (37)$$

Therefore, further integration over q or ω generically produces a logarithmic divergence at $\omega = \pm qv$, which stems from the collinear scattering $\phi_3 = \phi_1 = 0$ or π , see Eq. (34) at the light cone. This divergence reflects the fact that for a linear spectrum the momentum and energy conservation laws coincide in the ‘‘one-dimensional’’ collinear case. Note that this enhancement of the collinear scattering is not restricted to the case of undoped graphene.

In order to regularize this divergence, one has to go beyond the Golden-rule level and take into account the screening of the interaction (which in the clean case is perfect exactly on the light cone) and renormalization of the spectrum due to interaction (leading to nonlinear corrections). These mechanisms lead to the appearance of a large factor $|\ln(\alpha)| \gg 1$ in generic relaxation rates in graphene. In disordered graphene, this singularity is also cut off by disorder-induced broadening of the momentum-conservation delta-function.

C. Ansatz

The singularity in the collinear scattering in graphene leads to the fast thermalization of particles within given direction within each of the layers. Clearly, in an external electric field \mathbf{E} , the linearized nonequilibrium correction to the distribution function is proportional to the driving term $\mathbf{E}\mathbf{v}$. Therefore, the nonequilibrium correction

$$h_i(\epsilon, \mathbf{v}) = \chi(\epsilon) \frac{e\mathbf{E}\mathbf{v}}{T^2}$$

is characterized by some function of energy $\chi(\epsilon)$. One can formally expand this function in ϵ/T :

$$\chi(\epsilon) = \sum_{n=0}^{\infty} \chi_n(\epsilon/T)^n.$$

The action of the collision integral (which contains the combination $h_1 - h_2 + h_3 - h_4$) on this function generates the equilibration rate in all terms except for $n = 0, 1$. Indeed, for $n = 0$, the combination

$$h_1^{(0)} - h_2^{(0)} + h_3^{(0)} - h_4^{(0)} \propto \chi_0(\mathbf{v}_1 - \mathbf{v}_2 + \mathbf{v}_3 - \mathbf{v}_4)$$

contains the differences of velocities. This cancels the kinematics-induced divergency $\propto |\mathbf{v}_1 - \mathbf{v}_2 + \mathbf{v}_3 - \mathbf{v}_4|^{-1}$. For $n = 1$ the combination

$$h_1^{(1)} - h_2^{(1)} + h_3^{(1)} - h_4^{(1)} \propto \chi_1(\epsilon_1 \mathbf{v}_1 - \epsilon_2 \mathbf{v}_2 + \epsilon_3 \mathbf{v}_3 - \epsilon_4 \mathbf{v}_4) = \chi_1(\mathbf{p}_1 - \mathbf{p}_2 + \mathbf{p}_3 - \mathbf{p}_4) \quad (38)$$

contains the change of the total momentum of two colliding particles, which is exactly the argument of the momentum-conservation delta-function. All other contributions with $n > 1$ produce a relaxation rate enhanced by the collinear

scattering. The corresponding values of χ_n are therefore strongly suppressed compared to χ_0 and χ_1 , which justifies the following Ansatz [23]:

$$h_i(\epsilon, \mathbf{v}) = \left(\chi_\mu^i + \chi_T^i \frac{\epsilon - \mu}{T} \right) \frac{e\mathbf{E}\mathbf{v}}{T^2} = \left(\chi_0^i + \chi_1^i \frac{\epsilon}{T} \right) \frac{e\mathbf{E}\mathbf{v}}{T^2} \equiv \left(\chi_v^i + \chi_p^i \frac{\epsilon}{T} \right) \frac{e\mathbf{E}\mathbf{v}}{T^2}. \quad (39)$$

This correction to the distribution function contains only the two modes (proportional to velocity and momentum and characterized for each layer by the two constants $\chi_v = \chi_0$ and $\chi_p = \chi_1$, respectively), that nullify the collision integral in the case of collinear scattering. The notation χ_μ and χ_T is chosen to emphasize that, after the linearization with respect to \mathbf{E} , these quantities reflect the angular-dependent corrections to the chemical potential and temperature, respectively, in the direction-equilibrated distribution function:

$$n(\epsilon, \hat{\mathbf{v}}) = \frac{1}{1 + \exp\left[\frac{\epsilon - \mu(\hat{\mathbf{v}})}{2T(\hat{\mathbf{v}})}\right]} \simeq n_F(\epsilon) - \frac{\partial n_F(\epsilon)}{\partial \epsilon} \left[\frac{\delta\mu(\hat{\mathbf{v}})}{2T} + (\epsilon - \mu) \frac{\delta T(\hat{\mathbf{v}})}{2T^2} \right] \quad (40)$$

$$= n_F(\epsilon) - \frac{1}{2T} \frac{\partial n_F(\epsilon)}{\partial \epsilon} \left\{ \left[\delta\mu(\hat{\mathbf{v}}) - \frac{\mu}{T} \delta T(\hat{\mathbf{v}}) \right] + \frac{\epsilon}{T} \delta T(\hat{\mathbf{v}}) \right\}. \quad (41)$$

The Ansatz Eq. (39) greatly simplifies the solution of the kinetic equation, replacing the integral equation by a matrix one. Furthermore, the same kinematics-induced singularity in the collinear scattering as in I_{ii} appears in also the intralayer collision integrals I_{ij} . This implies fast unidirectional thermalization between the layers. Therefore, we set $\chi_T^{(1)} = \chi_T^{(2)}$, and hence reduce the kinetic equation for the double-layer setup to a 3×3 matrix equation (“three-mode approximation”).

D. Hydrodynamic equations

In each of the two layers, we introduce the particle currents (the total velocities)

$$\mathbf{J}_i = -NT \int d\epsilon \nu(\epsilon) \frac{\partial n_F^{(i)}}{\partial \epsilon} \int d\hat{\mathbf{v}} \mathbf{v} h_\alpha(\epsilon, \mathbf{v}), \quad (42)$$

and energy currents (or, equivalently, the total momenta)

$$\mathbf{P}_i = -N \int d\epsilon \nu(\epsilon) \epsilon \frac{\partial n_F^{(i)}}{\partial \epsilon} \int d\hat{\mathbf{v}} \mathbf{v} h_i(\epsilon, \mathbf{v}), \quad (43)$$

and substitute the Ansatz, Eq. 39, into these expressions, which yields

$$\mathbf{J}_i = \frac{N}{2} \left[A_0^{(i)} \chi_0^{(i)} + A_1^{(i)} \chi_1^{(i)} \right] \mathbf{E} \quad (44)$$

$$\mathbf{P}_i = \frac{N}{2} \left[A_1^{(i)} \chi_0^{(i)} + A_2^{(i)} \chi_1^{(i)} \right] \mathbf{E}. \quad (45)$$

Here

$$A_n^\alpha = -\frac{v^2}{T} \int d\epsilon \nu(\epsilon) \frac{\partial n_F^\alpha}{\partial \epsilon} \left(\frac{\epsilon}{T} \right)^n. \quad (46)$$

In terms of the currents, the fast interlayer thermalization ($\chi_T^{(1)} = \chi_T^{(2)}$) translates into the relation

$$B_2^b (\mathbf{P}_a - B_1^a \mathbf{J}_a) = B_2^a (\mathbf{P}_b - B_1^b \mathbf{J}_b), \quad (47)$$

where

$$B_0^\alpha = A_0^\alpha, \quad B_1^\alpha = \frac{A_1^\alpha}{A_0^\alpha}, \quad B_2^\alpha = A_2^\alpha - \frac{(A_1^\alpha)^2}{A_0^\alpha}. \quad (48)$$

The asymptotics of the functions $B_n^{(i)}(\mu_i/2T)$ read:

$$B_n^{(i)}(x \ll 1) = \begin{cases} \ln 2/\pi & n = 0 \\ 4x & n = 1 \\ 9\zeta(3)/2\pi & n = 2 \end{cases}, \quad B_n(x \gg 1) = \begin{cases} |x|/\pi & n = 0 \\ 2x & n = 1 \\ \pi|x|/3 & n = 2 \end{cases}. \quad (49)$$

It is also convenient to define $B_2 = B_2^{(1)} + B_2^{(2)}$. Finally, we introduce the total momentum (total energy current)

$$\mathbf{P} = \mathbf{P}_a + \mathbf{P}_b, \quad (50)$$

which is not affected by electron-electron collisions due to total momentum conservation in the e-e collision integral.

These transformations allow us to rewrite the matrix kinetic equation in the ‘‘hydrodynamic form’’. Here we can also introduce electric fields in both layers without doubling the number of relevant modes. Integrating the reduced matrix kinetic equation over the energy with

$$-NT \int d\epsilon_1 \nu(\epsilon) \frac{\partial n_F(\epsilon_1)}{\partial \epsilon_1} \{ \dots \} = N \int d\epsilon_1 \frac{\nu(\epsilon)}{\cosh^2 \frac{\epsilon_1 - \mu_i}{2T}} \{ \dots \} \quad (51)$$

and

$$-N \int d\epsilon_1 \epsilon_1 \nu(\epsilon) \frac{\partial n_F(\epsilon_1)}{\partial \epsilon_1} \{ \dots \} = N \int d\epsilon_1 \epsilon_1 \frac{\nu(\epsilon)}{\cosh^2 \frac{\epsilon_1 - \mu_i}{2T}} \{ \dots \} \quad (52)$$

yields the following steady-state equations (in order to avoid confusion in indices, from now on we label the layers by a and b)

$$\begin{aligned} \left\{ \frac{1}{\tau} + \left[(B_1^a)^2 + \frac{B_2}{B_0^a} \right] \frac{1}{\tau_{ee}^a} - B_1^a B_1^b \frac{1}{\tau_D} \right\} \mathbf{J}_a + \left\{ B_1^a B_1^b \frac{1}{\tau_{ee}^a} - \left[(B_1^b)^2 + \frac{B_2}{B_0^b} \right] \frac{1}{\tau_D} \right\} \mathbf{J}_b \\ = \frac{2}{N} T B_0^a e \mathbf{E}_a + \left(\frac{B_1^a}{\tau_{ee}^a} - \frac{B_1^b}{\tau_D} \right) \mathbf{P} \end{aligned} \quad (53)$$

$$\begin{aligned} \left\{ \frac{1}{\tau} + \left[(B_1^b)^2 + \frac{B_2}{B_0^b} \right] \frac{1}{\tau_{ee}^b} - B_1^a B_1^b \frac{1}{\tau_D} \right\} \mathbf{J}_b + \left\{ B_1^a B_1^b \frac{1}{\tau_{ee}^b} - \left[(B_1^a)^2 + \frac{B_2}{B_0^a} \right] \frac{1}{\tau_D} \right\} \mathbf{J}_a \\ = \frac{2}{N} T B_0^b e \mathbf{E}_b + \left(\frac{B_1^b}{\tau_{ee}^b} - \frac{B_1^a}{\tau_D} \right) \mathbf{P} \end{aligned} \quad (54)$$

$$\frac{\mathbf{P}}{\tau} = \frac{2}{N} T (B_0^a B_1^a e \mathbf{E}_a + B_0^b B_1^b e \mathbf{E}_b). \quad (55)$$

Here we have introduced the following effective transport relaxation rates:

$$\frac{1}{\tau_{ee}^a} = \frac{N}{8T^2 B_2} \int d\{\epsilon_i\} d\{\hat{\mathbf{v}}_i\} \left[(\mathbf{v}_1 - \mathbf{v}_2 + \mathbf{v}_3 - \mathbf{v}_4)^2 \mathcal{W}^{aa} + 2(\mathbf{v}_1 - \mathbf{v}_2)^2 \mathcal{W}^{ab} \right], \quad (56)$$

$$\frac{1}{\tau_{ee}^b} = \frac{N}{8T^2 B_2} \int d\{\epsilon_i\} d\{\hat{\mathbf{v}}_i\} \left[(\mathbf{v}_1 - \mathbf{v}_2 + \mathbf{v}_3 - \mathbf{v}_4)^2 \mathcal{W}^{bb} + 2(\mathbf{v}_1 - \mathbf{v}_2)^2 \mathcal{W}^{ba} \right], \quad (57)$$

$$\frac{1}{\tau_D} = \frac{N}{4T^2 B_2} \int d\{\epsilon_i\} d\{\hat{\mathbf{v}}_i\} (\mathbf{v}_1 - \mathbf{v}_2) (\mathbf{v}_4 - \mathbf{v}_3) \mathcal{W}^{ba}. \quad (58)$$

Here $1/\tau_{ee}^{a(b)}$ are the intralayer transport relaxation rates describing the velocity relaxation within a layer due to inelastic scattering with electrons in the same layer (described by \mathcal{W}^{aa}) and in the other layer (\mathcal{W}^{ab} term). The rate $1/\tau_D$ describes the interlayer velocity relaxation (velocity transfer from one layer to the other due to \mathcal{W}^{ab}): we call it the drag rate. The kernels \mathcal{W}^{ij} here are related to the kernel of the collision integral (23) as follows:

$$\mathcal{W}^{ij}(1, 2; 3, 4) = \frac{\nu(\epsilon_1)}{\cosh^2 \frac{\epsilon_1 - \mu_i}{2T}} W^{ij}(1, 2; 3, 4). \quad (59)$$

2. Ballistic regime

A. Resistivity matrix

The hydrodynamic equations (55) yield the following explicit expressions for the intralayer and interlayer resistivities:

$$\rho_{aa} = \frac{\hbar}{e^2} \frac{2B_2}{N(B_0^a)^2 T} \left[\frac{B_0^a}{\tau} + \frac{\frac{1}{\tau\tau_{ee}^a} + (B_1^b)^2 \left(\frac{1}{\tau_{ee}^a \tau_{ee}^b} - \frac{1}{\tau_D^2} \right)}{\frac{1}{\tau} + \frac{(B_1^a)^2}{\tau_{ee}^a} + \frac{(B_1^b)^2}{\tau_{ee}^b} - \frac{2B_1^a B_1^b}{\tau_D}} \right], \quad (60)$$

$$\rho_{ab} = -\frac{\hbar}{e^2} \frac{2B_2}{NB_0^a B_0^b T} \frac{\frac{1}{\tau\tau_D} + B_1^a B_1^b \left(\frac{1}{\tau_{ee}^a \tau_{ee}^b} - \frac{1}{\tau_D^2} \right)}{\frac{1}{\tau} + \frac{(B_1^a)^2}{\tau_{ee}^a} + \frac{(B_1^b)^2}{\tau_{ee}^b} - \frac{2B_1^a B_1^b}{\tau_D}} \quad (61)$$

$\rho_{bb} = \rho_{aa}(a \leftrightarrow b)$, and $\rho_{ba} = \rho_{ab}$. The drag coefficient is defined as

$$\rho_D = -\rho_{ab}. \quad (62)$$

It can also be rewritten in the following form,

$$\rho_D = \frac{\hbar}{e^2} \frac{2B_2}{NB_0^a B_0^b T \tau_D} \left[1 - \frac{\left(\frac{B_1^a}{\tau_{ee}^a} + \frac{B_1^b}{\tau_D} \right) \left(\frac{B_1^b}{\tau_{ee}^b} + \frac{B_1^a}{\tau_D} \right)}{\frac{1}{\tau_D} \left(\frac{1}{\tau} + \frac{(B_1^a)^2}{\tau_{ee}^a} + \frac{(B_1^b)^2}{\tau_{ee}^b} - \frac{2B_1^a B_1^b}{\tau_D} \right)} \right], \quad (63)$$

which for the disorder-dominated case yields directly the conventional perturbative drag:

$$\rho_D = \frac{\hbar}{e^2} \frac{2B_2}{NB_0^a B_0^b T \tau_D}. \quad (64)$$

For equal layers, we denote

$$\epsilon_0 = 2B_0 T/N, \quad C_1 = B_1, \quad C_2 = B_2/B_0. \quad (65)$$

Then the resistivity matrix reads

$$\hat{\rho} = \frac{\hbar}{e^2} \frac{C_2}{\epsilon_0} \left\{ \frac{1}{\tau} \begin{pmatrix} 1 & 0 \\ 0 & 1 \end{pmatrix} + \frac{C_2}{1/\tau + 2C_1^2(1/\tau_{ee} - 1/\tau_D)} \begin{pmatrix} 1/\tau_{ee} & -1/\tau_D \\ -1/\tau_D & 1/\tau_{ee} \end{pmatrix} \right. \\ \left. + \frac{C_2 C_1^2 (1/\tau_{ee} - 1/\tau_D^2)}{1/\tau + 2C_1^2(1/\tau_{ee} - 1/\tau_D)} \begin{pmatrix} 1 & -1 \\ -1 & 1 \end{pmatrix} \right\}. \quad (66)$$

Here the first term is the intralayer resistivity determined by disorder, the second term describes the conventional Coulomb drag in combination with the intralayer inelastic transport relaxation, and the last term arises due to the fast unidirectional thermalization in graphene.

In the clean limit $\tau = \infty$ the resistivity matrix has the form

$$\hat{\rho} = \frac{\hbar}{e^2} \frac{2B_2}{NT} \frac{\frac{1}{\tau_{ee}^a \tau_{ee}^b} - \frac{1}{\tau_D^2}}{\frac{(B_1^a)^2}{\tau_{ee}^a} + \frac{(B_1^b)^2}{\tau_{ee}^b} - \frac{2B_1^a B_1^b}{\tau_D}} \begin{pmatrix} \frac{(B_1^b)^2}{(B_0^a)^2} & -\frac{B_1^a B_1^b}{B_0^a B_0^b} \\ -\frac{B_1^a B_1^b}{B_0^a B_0^b} & \frac{(B_1^a)^2}{(B_0^b)^2} \end{pmatrix} \quad (67)$$

which for equal layers simplifies to

$$\hat{\rho} = \frac{\hbar}{e^2} \frac{C_2}{\epsilon_0} \left(\frac{1}{\tau_{ee}} + \frac{1}{\tau_D} \right) \begin{pmatrix} 1 & -1 \\ -1 & 1 \end{pmatrix}. \quad (68)$$

The off-diagonal component of this matrix is given in Eq. (14) of the main text.

B. Asymptotics of the drag coefficient

The general condition separating the disorder-dominated and Coulomb-dominated transport regimes can be found from Eq. (61), where one should compare the two terms in the numerator:

$$\frac{1}{\tau} \sim B_1^a B_1^b \tau_D \left(\frac{1}{\tau_{ee}^a \tau_{ee}^b} - \frac{1}{\tau_D^2} \right). \quad (69)$$

In the vicinity of the Dirac point ($\mu_{a,b} \ll T$), the intralayer transport relaxation rates are

$$\frac{1}{\tau_{ee}^{a,b}} \sim \alpha^2 NT, \quad (70)$$

whereas the drag rate was found in Ref. [16]:

$$\frac{1}{\tau_D} \sim \alpha^2 N \frac{\mu_a \mu_b}{T}, \quad (71)$$

so that $1/\tau_{ee} \gg 1/\tau_D$. Substituting these results into Eq. (69), we find

$$\frac{1}{\tau} \sim \frac{\mu_a \mu_b}{T^2} \frac{\tau_D}{\tau_{ee}^a \tau_{ee}^b} \sim \alpha^2 NT, \quad (72)$$

i.e. the crossover occurs at $1/\tau \sim 1/\tau_{ee}$.

Away from the Dirac point, $T \ll \mu_{a,b} \ll T/\alpha$, the drag rate is (for simplicity we set $\mu_a \sim \mu_b \sim \mu$)

$$\frac{1}{\tau_D} \sim \alpha^2 N \frac{T^2}{\mu} \ln \frac{\mu}{T}, \quad (73)$$

and

$$\frac{1}{\tau_{ee}} - \frac{1}{\tau_D} \sim \frac{1}{\tau_{ee}} \frac{T^2}{\mu^2} \ll \frac{1}{\tau_{ee}}. \quad (74)$$

It is worth mentioning that, for $\mu \gg T$, the intralayer scattering is much less efficient for the relaxation of velocity than the interlayer scattering. Indeed, the intralayer ($\propto \mathcal{W}^{ii}$) contribution to $1/\tau_{ee}$ in Eq. (58) contains the combination of velocities $\mathbf{v}_1 - \mathbf{v}_2 + \mathbf{v}_3 - \mathbf{v}_4$, which for $\mu \gg T$ is very close to $\mathbf{p}_1 - \mathbf{p}_2 + \mathbf{p}_3 - \mathbf{p}_4$. Therefore, at high chemical potentials $1/\tau_{ee}$ is dominated by the interlayer contribution ($\propto \mathcal{W}^{ab}$). Thus the crossover between the two regimes occurs for $\mu \gg T$ at

$$\frac{1}{\tau} \sim \frac{\mu^2}{T^2} \left(\frac{1}{\tau_{ee}} - \frac{1}{\tau_D} \right) \sim \alpha^2 N \frac{T^2}{\mu} \ln \frac{\mu}{T} \sim \frac{1}{\tau_{ee}}. \quad (75)$$

The drag coefficient in the disorder-dominated regime coincides with the perturbative result,

$$\begin{aligned} \rho_D &= \frac{\hbar}{e^2} \frac{2B_2}{NB_0^a B_0^b T \tau_D} \\ &\sim \frac{\hbar}{e^2} \alpha^2 \frac{T^2 (\mu_a + \mu_b)}{(\mu_a \mu_b)^2} \ln \frac{\min\{\mu_a, \mu_b\}}{T}, \quad T \ll \mu \ll \frac{T}{\alpha}, \quad \frac{1}{\tau} \gg \alpha^2 N \frac{T^2}{\mu}. \end{aligned} \quad (76)$$

In the opposite, ultraclean case, assuming for simplicity equal layers, we get from Eq. (68)

$$\begin{aligned} \rho_D &= \frac{\hbar}{e^2} \frac{C_2}{\epsilon_0} \left(\frac{1}{\tau_{ee}} + \frac{1}{\tau_D} \right) \simeq \frac{\hbar}{e^2} \frac{2C_2}{\epsilon_0 \tau_D} \\ &\sim \frac{\hbar}{e^2} \alpha^2 \frac{T^2}{\mu^2} \ln \frac{\mu}{T}, \quad T \ll \mu \ll \frac{T}{\alpha}, \quad \frac{1}{\tau} \ll \alpha^2 N \frac{T^2}{\mu}. \end{aligned} \quad (77)$$

The difference between the disordered (perturbative) and ultraclean (equilibrated) results for the drag is in the presence of $1/\tau_{ee}$ in the latter case. In particular, for equal layers, this enhances the drag by a factor of 2. Since these results are qualitatively the same, we do not analyze the behavior of the drag at yet higher chemical potentials, referring the reader to Ref. [16].

C. Third-order drag rate

It is important that the second-order (Golden-rule) drag rate vanishes at the Dirac point due to the particle-hole symmetry. However, the particle-hole symmetry does not affect the odd-order drag rates [29]. Near the Dirac point, such rates should not depend on μ and hence are proportional to T . Taking into account the second-order matrix element $M_{ab}^{(2)} \propto \alpha^2$,

$$\left| M_{ab}^{(1)} + M_{ab}^{(2)} \right|^2 \simeq \left| M_{ab}^{(1)} \right|^2 + 2\text{Re} \left\{ M_{ab}^{(1)} \left[M_{ab}^{(2)} \right]^* \right\}, \quad (78)$$

we estimate

$$\frac{1}{\tau_D} \sim \alpha^2 N \frac{\mu^2}{T^2} + \alpha^3 NT, \quad (79)$$

where we skip the numerical prefactors in both terms. A similar correction arises in $1/\tau_{ee}$, but there it is always subleading for $\alpha \ll 1$. Substituting this correction into Eq. (66), we find

$$\rho_D \sim \frac{\hbar}{e^2} \frac{1}{NT} \frac{\frac{N}{\tau} \left(\alpha^2 \frac{\mu^2}{T^2} + \alpha^3 T \right) + \frac{\mu^2 N^2}{T^2} \left[\alpha^4 T^2 - \left(\alpha^2 \frac{\mu^2}{T^2} + \alpha^3 T \right)^2 \right]}{\frac{1}{\tau} + \frac{\mu^2 N}{T^2} \left[\alpha^2 T + \left(\alpha^2 \frac{\mu^2}{T^2} + \alpha^3 T \right) \right]} \quad (80)$$

Clearly, for $\mu \gg \alpha^{1/2} T$ we can disregard the α^3 -terms. In the opposite limit, we neglect the conventional drag term:

$$\rho_D \sim \frac{\hbar}{e^2} \frac{\alpha^3 T + \alpha^4 \mu^2 \tau N}{T + \alpha^2 \mu^2 \tau N}, \quad \mu \ll \alpha^{1/2} T, \quad \frac{1}{\tau} \ll T. \quad (81)$$

Exactly at the Dirac point this yields

$$\rho_D \sim \frac{\hbar}{e^2} \alpha^3. \quad (82)$$

For finite chemical potential, this result is valid for

$$\frac{1}{\tau} \gg \alpha N \frac{\mu^2}{T}. \quad (83)$$

In the opposite limit, one can neglect the α^3 -term, yielding

$$\rho_D \sim \frac{\hbar}{e^2} \frac{\alpha^4 \mu^2 \tau N}{T + \alpha^2 \mu^2 \tau N} = \frac{\hbar}{e^2} \begin{cases} \alpha^2, & 1/\tau \ll \alpha^2 N \mu^2 / T \\ \alpha^4 N \mu^2 \tau / T, & \alpha^2 N \mu^2 / T \ll 1/\tau \ll \alpha N \mu^2 / T \end{cases}. \quad (84)$$

3. Diffusive regime

A. Third-order contribution to the drag

In this section we analyze the third-order drag [29] in the diffusive regime $T\tau \ll 1$ for the case of high dimensionless conductances (per spin and per valley), $g = \nu D \sim \mu\tau \gg 1$, where $D = v^2\tau/2$ is the diffusion coefficient. In this limit, one can calculate the prefactor analytically. In the vicinity of the Dirac point $\mu\tau \ll 1$, the conductance is of order unity. Indeed, experiments on high-quality samples show T -independent σ down to $T = 30$ mK [31], that can be explained by the specific character of disorder in graphene [32]. Therefore, there we also assume the diffusive dynamics described by the diffusion propagators

$$\mathcal{D}_i(q, \omega) = \frac{1}{\nu_i} \frac{1}{D_i q^2 - i\omega}, \quad qv, \omega \ll 1/\tau, \quad (85)$$

and polarization operators

$$\Pi_i(q, \omega) = N\nu_i \frac{D_i q^2}{D_i q^2 - i\omega}, \quad (86)$$

where ν_i is the density of states of the layer (per spin and valley) $i = 1, 2$ and D_i is its diffusion coefficient.

The third-order drag resistivity was calculated in Ref. [29] for the case of large interlayer distance, $\kappa d \gg 1$. Here we generalize this result to the opposite case $\kappa d \ll 1$, which is experimentally relevant for graphene near the Dirac point.

The analytic expression for the third-order drag resistivity is given by [29]

$$\begin{aligned} \rho_D^{(3)} &= \frac{\hbar}{e^2} 32Tg_1g_2 \int_0^\infty d\omega d\Omega \mathcal{F}_1(\omega, \Omega) \mathcal{F}_2(\omega, \Omega) \\ &\times \int \frac{d^2q}{(2\pi)^2} \int \frac{d^2Q}{(2\pi)^2} \text{Im} \left[\mathcal{D}_1(q, \omega) \mathcal{D}_2(q, \omega) \mathcal{V}_{12}(q, \omega) \mathcal{V}_{12} \left(\frac{\mathbf{q}}{2} - \mathbf{Q}, \frac{\omega}{2} - \Omega \right) \mathcal{V}_{12} \left(\frac{\mathbf{q}}{2} + \mathbf{Q}, \frac{\omega}{2} + \Omega \right) \right]. \end{aligned} \quad (87)$$

Here the thermal factors $\mathcal{F}_i(\omega, \Omega)$ are given by

$$\mathcal{F}_1(\omega, \Omega) = T \frac{\partial}{\partial \Omega} [\mathcal{B}(\Omega + \omega/2) - \mathcal{B}(\Omega - \omega/2)], \quad (88a)$$

$$\mathcal{F}_2(\omega, \Omega) = 2 - \mathcal{B}(\Omega + \omega/2) - \mathcal{B}(\Omega - \omega/2) + \mathcal{B}(\omega), \quad (88b)$$

where

$$\mathcal{B}(\omega) = \frac{\omega}{T} \coth \left(\frac{\omega}{2T} \right). \quad (88c)$$

The propagators of longitudinal vector potentials $\mathcal{V}_{12}(q, \omega)$ in Eq. (87) include the dressing of the vertices by diffusons:

$$\mathcal{V}_{12}(q, \omega) = \frac{q^2 U_{12}^{\text{RPA}}(q, \omega)}{(D_1 q^2 - i\omega)(D_2 q^2 - i\omega)}, \quad (89)$$

where the retarded RPA-screened interlayer interaction $U_{12}^{\text{RPA}}(q, \omega)$ is defined in Eq. (29).

For simplicity, we consider equal layers. For small interlayer distance $d \ll v\tau$ we have $qd \ll 1$. It is convenient to introduce the inverse screening length

$$\kappa = 2\pi e^2 \nu, \quad (90)$$

where ν is the thermodynamic density of states per one flavor of particles. Expanding $\exp(-qd) \simeq 1 - qd$ we get

$$\begin{aligned} U_{12}^{\text{RPA}}(q, \omega) &= U_{12}^{(0)}(q) \left[\left(1 + U_{11}^{(0)}(q) \Pi(q, \omega) \right)^2 - \left(U_{12}^{(0)}(q) \Pi(q, \omega) \right)^2 \right]^{-1} \\ &= \frac{1}{\nu} \frac{\kappa e^{-qd}}{q} \left[\left(1 + \frac{N\kappa}{q} \frac{Dq^2}{Dq^2 - i\omega} \right)^2 - \left(\frac{N\kappa e^{-qd}}{q} \frac{Dq^2}{Dq^2 - i\omega} \right)^2 \right]^{-1} \\ &\simeq \frac{1}{\nu} \frac{\kappa}{q} \frac{(Dq^2 - i\omega)^2}{[Dq(q + 2N\kappa) - i\omega][Dq^2(1 + N\kappa d) - i\omega]}, \end{aligned} \quad (91)$$

and hence

$$\mathcal{V}_{12}(q, \omega) = \frac{1}{\nu} \frac{\kappa q}{[Dq(q + 2N\kappa) - i\omega][Dq^2(1 + N\kappa d) - i\omega]}. \quad (92)$$

We first consider the case of large interlayer separation, $N\kappa d \gg 1$. For $N\kappa \gg \max\{1/d, (T/D)^{1/2}\}$ we find

$$\mathcal{V}_{12}(q, \omega) \simeq \frac{1}{2Ng} \frac{1}{Dq^2 N\kappa d - i\omega}, \quad (93)$$

which reproduces the result of Ref. [29]:

$$\rho_D^{(3)} \sim \frac{\hbar}{e^2} \frac{1}{N^3 g^3} \frac{1}{(N\kappa d)^2}. \quad (94)$$

For $1/d \ll N\kappa \ll (T/D)^{1/2}$,

$$\mathcal{V}_{12}(q, \omega) \simeq \frac{1}{\nu} \frac{\kappa q}{Dq^2 - i\omega} \frac{1}{Dq^2 N\kappa d - i\omega}, \quad (95)$$

and we find

$$\rho_D^{(3)} \sim \frac{\hbar}{e^2} \frac{1}{g^3} \frac{1}{(N\kappa d)^2} \left(\frac{D\kappa^2}{T} \right)^{3/2}. \quad (96)$$

In the opposite case $N\kappa d \ll 1$ (which is relevant to our problem),

$$\mathcal{V}_{12}(q, \omega) \simeq \frac{1}{\nu} \frac{\kappa q}{[Dq(q + 2N\kappa) - i\omega] [Dq^2 - i\omega]}. \quad (97)$$

Substituting this into Eq. (87), we get

$$\begin{aligned} \rho_D^{(3)} &= \frac{\hbar}{e^2} 32T \frac{g^2}{\nu^5} \int_0^\infty d\omega d\Omega \mathcal{F}_1(\omega, \Omega) \mathcal{F}_2(\omega, \Omega) \int \frac{d^2 q}{(2\pi)^2} \int \frac{d^2 Q}{(2\pi)^2} \text{Im} \left\{ \left[\frac{1}{Dq^2 - i\omega} \right]^2 \frac{\kappa q}{[Dq(q + 2N\kappa) - i\omega][Dq^2 - i\omega]} \right. \\ &\times \frac{\kappa|\mathbf{q}/2 - \mathbf{Q}|}{[D(\mathbf{q}/2 - \mathbf{Q})^2 + 2D|\mathbf{q}/2 - \mathbf{Q}|N\kappa - i(\omega/2 - \Omega)] [D(\mathbf{q}/2 - \mathbf{Q})^2 - i(\omega/2 - \Omega)]} \\ &\times \left. \frac{\kappa|\mathbf{q}/2 + \mathbf{Q}|}{[D(\mathbf{q}/2 + \mathbf{Q})^2 + 2D|\mathbf{q}/2 + \mathbf{Q}|N\kappa - i(\omega/2 + \Omega)] [D(\mathbf{q}/2 + \mathbf{Q})^2 - i(\omega/2 + \Omega)]} \right\}. \end{aligned} \quad (98)$$

The frequency integrals are dominated by $\omega \sim \Omega \sim T$, whereas the momentum integrals are dominated by $q \sim Q \sim q_T = \sqrt{T/D}$. Therefore, the drag conductivity in Eq. (98) can be estimated as

$$\begin{aligned} \rho_D^{(3)} &\sim \frac{\hbar}{e^2} \frac{Tg^2}{\nu^5} \underbrace{T^2}_{d\omega d\Omega} \underbrace{q_T^4}_{d^2 q d^2 Q} \frac{1}{(Dq_T^2 + T)^5} \frac{\kappa^3 q_T^3}{(Dq_T^2 + T + Dq_T N\kappa)^3} \\ &\sim \frac{\hbar}{e^2} \frac{1}{g^3} \left(\frac{\kappa}{N\kappa + \sqrt{T/D}} \right)^3. \end{aligned} \quad (99)$$

Therefore, for $N\kappa \gg \sqrt{T/D}$ we get

$$\rho_D^{(3)} \sim \frac{\hbar}{e^2} \frac{1}{N^3 g^3}, \quad (100)$$

while for $N\kappa \ll \sqrt{T/D}$ we find

$$\rho_D^{(3)} \sim \frac{\hbar}{e^2} \frac{1}{g^3} \left(\frac{D\kappa^2}{T} \right)^{3/2}. \quad (101)$$

In the first case the expression for the third-order drag coefficient is given by

$$\begin{aligned} \rho_D^{(3)} &= \frac{\hbar}{e^2} 32T \frac{g^2}{\nu^5} \int_0^\infty d\omega d\Omega \mathcal{F}_1(\omega, \Omega) \mathcal{F}_2(\omega, \Omega) \int \frac{d^2 q}{(2\pi)^2} \int \frac{d^2 Q}{(2\pi)^2} \text{Im} \left\{ \left[\frac{1}{Dq^2 - i\omega} \right]^2 \right. \\ &\times \left. \left(\frac{1}{2ND} \right)^3 \frac{1}{Dq^2 - i\omega} \frac{1}{D(\mathbf{q}/2 - \mathbf{Q})^2 - i(\omega/2 - \Omega)} \frac{1}{D(\mathbf{q}/2 + \mathbf{Q})^2 - i(\omega/2 + \Omega)} \right\}. \end{aligned} \quad (102)$$

The integrals here are now dimensionless [one measures momenta in units of $(T/D)^{1/2}$ and frequencies in units of T]. In the second case the prefactor is again determined by a dimensionless integral:

$$\begin{aligned} \rho_D^{(3)} &= \frac{\hbar}{e^2} 32T \frac{g^2}{\nu^5} \int_0^\infty d\omega d\Omega \mathcal{F}_1(\omega, \Omega) \mathcal{F}_2(\omega, \Omega) \int \frac{d^2q}{(2\pi)^2} \int \frac{d^2Q}{(2\pi)^2} \text{Im} \left\{ \left[\frac{1}{Dq^2 - i\omega} \right]^2 \right. \\ &\quad \left. \times \kappa^3 \frac{q}{[Dq^2 - i\omega]^2} \frac{|\mathbf{q}/2 - \mathbf{Q}|}{[D(\mathbf{q}/2 - \mathbf{Q})^2 - i(\omega/2 - \Omega)]^2} \frac{|\mathbf{q}/2 + \mathbf{Q}|}{[D(\mathbf{q}/2 + \mathbf{Q})^2 - i(\omega/2 + \Omega)]^2} \right\}. \end{aligned} \quad (103)$$

For $T\tau \ll 1$ and $\mu\tau \gg 1$, we have

$$\kappa \sim \alpha\mu/v, \quad (104)$$

which implies

$$N\kappa = \sqrt{\frac{T}{D}} \leftrightarrow \frac{1}{\tau} = \frac{\alpha^2 N^2 \mu^2}{T}. \quad (105)$$

For $\mu\tau \ll 1$, we have

$$\kappa \sim \alpha/v\tau, \quad (106)$$

and hence

$$N\kappa = \sqrt{\frac{T}{D}} \leftrightarrow \frac{1}{\tau} = \frac{T}{\alpha^2 N^2}. \quad (107)$$

Thus, for

$$\max\{T, \alpha^2 N^2 \mu^2 / T\} \ll 1/\tau \ll T/\alpha^2 N^2$$

the third-order drag resistivity reads:

$$\rho_D^{(3)} \sim \frac{\alpha^3}{(T\tau)^{3/2}}. \quad (108)$$

At $T\tau \sim 1$ this result matches the ballistic third-order drag resistivity, Eq. (82).

For yet lower $T \ll \alpha^2 N^2 / \tau$ and $\mu\tau \ll 1$ the third-order drag saturates at

$$\rho_D^{(3)} \sim \frac{\hbar}{e^2} \frac{1}{N^3}. \quad (109)$$

Finally, for $\mu\tau \gg \max\{1, (T\tau)^{1/2}/\alpha N\}$, the third-order drag behaves as

$$\rho_D^{(3)} \sim \frac{\hbar}{e^2} \frac{1}{(N\mu\tau)^3}. \quad (110)$$

4. Correlated disorder

In the original version of the paper we mentioned the correlations between the disorder potentials of the two layers [34] as an alternative mechanism leading to a low- T peak in ρ_D at the Dirac point. After the submission of the original version, we became aware of a preprint by Song and Levitov [35] that focused on such a mechanism. In this section we analyze the role of interlayer correlations of disorder potentials (both of short-range and long-range nature) within our general framework. This allows us to compare the effect of correlated disorder with the third-order drag considered in the main text and in Sections 2C and 3 of the Supplemental Material.

As emphasized in Ref. [35], the correlations between the disorder potentials of the two layers might be especially important in drag experiments on graphene near the Dirac point for the two reasons: (i) similarly to the third-order drag, it does not require [34] the particle-hole symmetry and hence provides finite drag at the charge neutrality point [35]; (ii) in contrast to experiments on conventional semiconducting double wells, the interlayer distance in graphene experiments is rather small, which enhances the disorder correlations between the layers. In what follows, we analyze the two models of correlations: (A) Correlated scattering off common short-range impurities [34] and (B) correlations of large-scale inhomogeneities of the chemical potentials in the layers [35].

A. Short-range correlations: correlated impurity scattering

Following Ref. [34], we introduce the matrix of disorder correlators $w_{\hat{\mathbf{v}}\hat{\mathbf{v}}'}^{(ij)} = \langle u^{(i)}u^{(j)} \rangle_{\text{imp}}$. The values of $w^{(ij)}$ at $i \neq j$ differ from zero due to correlations between the impurity potentials $u^{(i)}$ in different layers. The total scattering rates are defined by

$$\frac{1}{\tau_{ij}} = \left\langle w_{\hat{\mathbf{v}}\hat{\mathbf{v}}'}^{ij} \frac{1 + \hat{\mathbf{v}}\hat{\mathbf{v}}'}{2} \right\rangle, \quad (111)$$

where the symbol $\langle \dots \rangle$ stands for the angular average. The disorder correlations between the layers are described by the characteristic rate

$$\frac{1}{\tau_g} = \frac{\tau_{12} - \tau}{\tau^2}, \quad (112)$$

where $1/\tau = [1/\tau_{11} + 1/\tau_{22}]/2$. The time scale τ_g is a characteristic scale on which carriers in the two layers start “feeling” the difference between the impurity potentials $u^{(1)}$ and $u^{(2)}$. The potentials in the two layers are strongly correlated when $\tau_g \gg \tau$. One might expect that for realistic systems the situation of moderately correlated potentials, $\tau_g \sim \tau \sim \tau_{12}$, is typically realized. Weakly correlated potentials ($\tau_{12} \gg \tau$) yield $\tau_g \ll \tau$. Below we assume that disorder is sufficiently short-ranged and do not distinguish between the total and transport scattering rates for the estimates.

We start from the ballistic regime $T\tau \gg 1$. The correlated disorder affects the drag in a way similar to the third-order drag. With correlated disorder, one can include an interlayer disorder line w_{12} into the inelastic scattering amplitude. In the ballistic $\rho_D^{(3)}$ drag we had one amplitude M_2 with two interaction lines and one with a single wave line (M_1). The corresponding drag rate contains $2Re[M_1(M_2)^*] \propto \alpha^3$. Now one can form the second-order scattering amplitude M_2 using one interaction line (α) and one interlayer-disorder line, which introduces a factor $(T\tau_{12})^{-1}$. This gives

$$\frac{1}{\tau_D^{\text{corr}}} \sim \alpha^2 T (T\tau_{12})^{-1} = \alpha^2 / \tau_{12}, \quad (113)$$

and

$$\rho_D^{\text{corr}} \sim \frac{\alpha^2}{T\tau_{12}}, \quad (114)$$

which overcomes the third-order drag $\rho_D^{(3)} \sim \alpha^3$ for $1/\tau_{12} > \alpha T$. This happens in the perturbative regime ($1/\tau > \alpha^2 T$, assuming correlated disorder, $\tau_{12} \sim \tau$), where the correlated-disorder contribution can be calculated diagrammatically. Similarly to $\sigma_D^{(3)}$, the corresponding diagram involves two four-leg vertices (hence finite drag at the Dirac point $\mu = 0$), but now connected in all possible ways by two interaction lines and one disorder line w_{12} .

The general expression for the drag resistivity in the ballistic regime, including both third-order and correlated-disorder drag rates for equal layers has the form:

$$\rho_D \sim \frac{\hbar}{e^2} \frac{1}{NT} \frac{\frac{N}{\tau} \left(\alpha^2 \frac{\mu^2}{T^2} + \alpha^3 T + \frac{\alpha^2}{T\tau_{12}} \right) + \frac{\mu^2 N^2}{T^2} \left[\alpha^4 T^2 - \left(\alpha^2 \frac{\mu^2}{T^2} + \alpha^3 T + \frac{\alpha^2}{T\tau_{12}} \right)^2 \right]}{\frac{1}{\tau} + \frac{\mu^2 N}{T^2} \left[\alpha^2 T + \left(\alpha^2 \frac{\mu^2}{T^2} + \alpha^3 T + \frac{\alpha^2}{T\tau_{12}} \right) \right]} \quad (115)$$

Exactly at the Dirac point it reduces to:

$$\rho_D(\mu = 0) \sim \frac{\hbar}{e^2} \alpha^2 \left(\frac{1}{T\tau_{12}} + \alpha \right). \quad (116)$$

Let us now analyze the role of correlated disorder in the diffusive regime $T\tau \ll 1$. Again, we assume the absence of localization at the Dirac point (see Section 3). The drag resistivity for the case of correlated disorder was calculated in the diffusive regime in Ref. [34]. It is dominated by the Maki-Thompson diagram with an interlayer Cooper propagator. It is worth noting that any difference in the disorder potentials (as well as in chemical potentials of the layers) leads to a finite gap in these propagators given by $1/\tau_g$. The main result of Ref. [34] is as follows:

$$\rho_D^{\text{corr}} \sim \frac{\hbar}{e^2} \frac{1}{g^2 [\lambda_{21}^{-1} + \ln(\varepsilon_0/T)]^2} \ln \frac{T\tau_\varphi\tau_g}{\tau_\varphi + \tau_g} \quad (117)$$

at $\tau_g^{-1} \ll T \ll \tau^{-1}$, and

$$\rho_D^{\text{corr}} \sim \frac{\hbar}{e^2} \frac{(T\tau_g)^2}{g^2 [\lambda_{21}^{-1} + \ln(\varepsilon_0\tau_g)]^2}. \quad (118)$$

at lower temperatures $T \ll \tau_g^{-1}$.

In graphene near the Dirac point, for small interlayer distance $\kappa d \ll 1$ the interlayer interaction constant in the Cooper channel is $\lambda_{12} \sim \alpha$. The Cooper channel cutoff energy is $\epsilon_0 = 1/\tau$ (the logarithm in the Cooper channel appears only for a constant density of states; in graphene in the diffusive regime this happens only for energies below $1/\tau$), the dimensionless conductance $g \sim 1$, and $\tau_\phi \sim 1/T$. Substituting these values to Eqs. (117) and (118), we arrive at

$$\rho_D^{\text{corr}} \sim \frac{\hbar}{e^2} \frac{\alpha^2}{[1 - \alpha \ln(T\tau)]^2}, \quad \tau_g^{-1} \ll T \ll \tau^{-1}, \quad (119)$$

$$\rho_D^{\text{corr}} \sim \frac{\hbar}{e^2} \frac{\alpha^2 (T\tau_g)^2}{[1 - \alpha \ln(T\tau)]^2}, \quad T \ll \tau_g^{-1}. \quad (120)$$

These results are $\propto \alpha^2$ for realistic temperatures, $T\tau \gg \exp(-1/\alpha)$. For a moderately correlated disorder $\tau_g \sim \tau$, Eqs. (114) and (120) then lead to

$$\rho_D^{\text{corr}} \sim \frac{\hbar}{e^2} \alpha^2 \begin{cases} (T\tau)^{-1}, & T\tau \gg 1 \\ (T\tau)^2, & T\tau \ll 1 \end{cases}, \quad (121)$$

which yields a maximum at $T \sim 1/\tau$ in the temperature dependence of the drag resistivity at the charge neutrality point. For strongly correlated disorder potentials ($\tau_g \gg \tau$), this maximum develops into a plateau between $\tau_g^{-1} \ll T \ll \tau^{-1}$.

B. Long-range correlations: correlated macroscopic inhomogeneities

Let us now analyze within our kinetic-equation framework the model of correlated macroscopic spatial fluctuations $\delta\mu_i$ in chemical potentials of the two layers [35], characterized by the correlation function

$$F_{ij}^{(\mu)}(\mathbf{r} - \mathbf{r}') = \langle \delta\mu_i(\mathbf{r}) \delta\mu_j(\mathbf{r}') \rangle \neq 0. \quad (122)$$

We restrict ourselves to the ballistic regime $T\tau \gg 1$. Assuming the spatial scale of the fluctuations to be much larger than all characteristic scales related to the particle scattering, $v\tau_{ee}$, $v\tau_D$, and $v\tau$, we solve the hydrodynamic equations locally, yielding Eq. (61) with local values of the chemical potentials encoded in functions $B_1^{(a,b)} \sim \mu_{a(b)}/T$, as well as in the local drag rate

$$\frac{1}{\tau_D(\mathbf{r})} \sim \alpha^2 N \frac{\mu_1(\mathbf{r})\mu_2(\mathbf{r})}{T}.$$

On the other hand, since the coefficients $B_0 \sim 1$ and $B_2 \sim 1$, as well as the transport electron-electron scattering rate $\tau_{ee}^{-1} \sim \alpha^2 T$ are finite at the neutrality point, we can neglect the fluctuations of μ_i in these quantities. Exactly at the Dirac point $\mu_{1,2} = 0$, assuming that the fluctuations of chemical potentials are weak (the precise condition is established below), we can further neglect the B_1 -terms in the denominator of Eq. (61), yielding for the ‘‘local resistivity’’

$$\begin{aligned} \rho_D(\mathbf{r}) &\simeq \frac{\hbar}{e^2} \frac{2B_2\tau}{NB_0^a B_0^b T} \left[\frac{1}{\tau\tau_D(\mathbf{r})} + \frac{B_1^a(\mathbf{r})B_1^b(\mathbf{r})}{\tau_{ee}^a \tau_{ee}^b} \right] \\ &\sim \frac{\hbar}{e^2} \frac{\tau}{NT} \delta\mu_1(\mathbf{r})\delta\mu_2(\mathbf{r}) \left(\frac{\alpha^2 N}{T\tau} + \alpha^4 N^2 \right). \end{aligned} \quad (123)$$

Averaging this expression over the small fluctuations of the correlated chemical potentials [35], we arrive at the correction to the universal third-order result, $\rho_D^{(3)}(\mu = 0) \sim (\hbar/e^2)\alpha^3$,

$$\Delta\rho_D(\mu = 0) \sim \frac{\hbar}{e^2} \frac{\alpha^2 F_{12}^{(\mu)}(0)}{T^2} (1 + \alpha^2 NT\tau) \sim \frac{\hbar}{e^2} \frac{F_{12}^{(\mu)}(0)}{T^2} \begin{cases} \alpha^4 NT\tau & \frac{1}{\tau} \ll \alpha^2 NT, \\ \alpha^2 & \alpha^2 NT \ll \frac{1}{\tau} \ll T. \end{cases} \quad (124)$$

We see that in the Coulomb-dominated transport regime, this correction is dominated by the fluctuations in B_1 , whereas in the disorder-dominated (perturbative) regime, the main role is played by a locally finite drag rate.

Finally, in the ultraclean limit

$$\frac{1}{\tau} \ll \alpha^2 N F_{ii}^{(0)} / T, \quad (125)$$

we can neglect $1/\tau$ in the denominator of the local drag resistivity given by Eq. (61), yielding a natural analog of Eq. (15):

$$\Delta\rho_D(\mu=0)(\mathbf{r}) \sim \frac{\hbar}{e^2} \alpha^2 \frac{\delta\mu_1 \delta\mu_2}{\delta\mu_1 \delta\mu_1 + \delta\mu_2 \delta\mu_2}. \quad (126)$$

In particular, for perfectly correlated chemical potentials, $\delta\mu_1(\mathbf{r}) = \delta\mu_2(\mathbf{r})$, the fluctuations drops out from Eq. (126) and the local resistivity turns out to be independent of \mathbf{r} . In a more general case, the averaging over fluctuations becomes nontrivial, but this can only affect the numerical prefactor in the final result. Thus, the correlated large-scale fluctuations of the chemical potentials in the layers in effect shift the curve 1 in Fig. 2 upwards, extending the validity of the fully equilibrated result,

$$\rho_D \sim \frac{\hbar}{e^2} \alpha^2, \quad (127)$$

to the case of finite disorder, Eq. (125), at the Dirac point. This implies that in the case of correlated inhomogeneities the disorder-induced dip in the lower left panel of Fig. 1 develops only for sufficiently strong disorder.

-
- [1] A.G. Rojo, J. Phys.: Condens. Matter, **11** R31 (1999).
[2] P.M. Solomon *et al.*, Phys. Rev. Lett. **63**, 2508 (1989); T.J. Gramila *et al.*, Phys. Rev. Lett. **66**, 1216 (1991).
[3] D. Snoke, Science **298**, 1368 (2002).
[4] M. Yamamoto *et al.*, Science **313**, 204 (2006).
[5] R. Pilarisetty *et al.*, Phys. Rev. B **71**, 115307 (2002).
[6] A.S. Price *et al.*, Science **316**, 99 (2007).
[7] S. Kim *et al.*, Phys. Rev. B **83**, 161401(R) (2011).
[8] E. Tutuc and S. Kim, Solid State Commun. (2012).
[9] A.K. Geim, K.S. Novoselov, and L. Ponomarenko, private communication.
[10] A. Kamenev and Y. Oreg, Phys. Rev. B **52**, 7516 (1995).
[11] A.-P. Jauho and H. Smith, Phys. Rev. B, **47** 4420 (1993); K. Flensberg *et al.*, Phys. Rev. B **52**, 14761 (1995).
[12] B.N. Narozhny, Phys. Rev. B **76**, 153409 (2007).
[13] W. Tse, Ben Yu-Kaang Hu, and S. Das Sarma, Phys. Rev. B **76**, 081401 (2007).
[14] N.M.R. Peres, J.M.B. Lopes dos Santos, and A.H. Castro Neto, Europhys. Lett. **95** 18001 (2011).
[15] E.H. Hwang, R. Sensarma, S. Das Sarma, Phys. Rev. B **84**, 245441 (2011).
[16] B.N. Narozhny *et al.*, Phys. Rev. B **85**, 195421 (2012).
[17] For a detailed overview of the existing literature on the Coulomb drag in graphene see M. Carrega, T. Tudorovskiy, A. Principi, M.I. Katsnelson, and M. Polini, arXiv:1203.3386 (unpublished).
[18] S.M. Badalyan and F.M. Peeters, arXiv:1112.5886; arXiv:1204.4598 (unpublished).
[19] B. Amorim, N.M.R. Peres, arXiv:1203.6777 (unpublished).
[20] B. Scharf and A. Matos-Abiague, arXiv:1204.3385 (unpublished).
[21] Related effect of photon drag in graphene was investigated in J. Karch *et al.*, Phys. Rev. Lett. **105** 227402 (2010).
[22] L. Ponomarenko *et al.*, Nature Physics **7**, 958 (2011).
[23] A.B. Kashuba, Phys. Rev. B **78**, 085415 (2008).
[24] L. Fritz *et al.*, Phys. Rev. B **78**, 085416 (2008); M. Müller, J. Schmalian, and L. Fritz, Phys. Rev. Lett. **103**, 025301 (2009).
[25] D. Svintsov *et al.*, arXiv:1201.0592 (unpublished).
[26] We treat impurity scattering within the relaxation time approximation assuming energy-independent transport time τ . Generalization onto the more realistic case of Coulomb impurities with the energy-dependent transport time is straightforward and does not qualitatively affect the results.
[27] See Supplemental Material for details of the quantum kinetic equation and estimates for the third-order drag in the diffusive regime.
[28] M. Schütt, P.M. Ostrovsky, I.V. Gornyi, A.D. Mirlin, Phys. Rev. B **83**, 155441 (2011).
[29] A. Levchenko and A. Kamenev, Phys. Rev. Lett. **100**, 026805 (2008).
[30] B.N. Narozhny, I.L. Aleiner, and A. Stern, Phys. Rev. Lett. **86**, 3610 (2001).
[31] Y.-W. Tan *et al.*, Eur. Phys. J. Special Topics **148**, 15 (2007).
[32] P.M. Ostrovsky, I.V. Gornyi, and A.D. Mirlin, Phys. Rev. B **74**, 235443 (2006); Phys. Rev. Lett. **98**, 256801 (2007); Eur. Phys. J. Spec. Top. **148**, 63 (2007).
[33] M.P. Mink *et al.*, Phys. Rev. Lett. **108**, 186402 (2012).
[34] I.V. Gornyi, A.G. Yashenkin, and D.V. Khveshchenko, Phys. Rev. Lett. **83**, 152 (1999).
[35] J.C.W. Song and L.S. Levitov, arXiv:1205.5257 (unpublished).
[36] J. Lux and L. Fritz, (unpublished).